
OPTIMIZING DATA TRANSFER PERFORMANCE AND ENERGY EFFICIENCY WITH DEEP REINFORCEMENT LEARNING

Hasubil Jamil

Department of Computer Science and Engineering
University at Buffalo, Buffalo, NY
mdhasibu@buffaloe.edu

Jacob Goldverg

Department of Computer Science and Engineering
University at Buffalo, Buffalo, NY
jacobgol@buffaloe.edu

Elvis Rodrigues

Department of Computer Science and Engineering
University at Buffalo, Buffalo, NY
elvisdav@buffaloe.edu

MD S Q Zulkar Nine

Department of Computer Science
Tennessee Tech University, Cookeville, TN
mnine@tntech.edu

Tevfik Kosar

Department of Computer Science and Engineering
University at Buffalo, Buffalo, NY
tkosar@buffaloe.edu

March 19, 2025

ABSTRACT

The rapid growth of data across fields of science and industry has increased the need to improve the performance of end-to-end data transfers while using the resources more efficiently. In this paper, we present a dynamic, multiparameter reinforcement learning (RL) framework that adjusts application-layer transfer settings during data transfers on shared networks. Our method strikes a balance between high throughput and low energy utilization by employing reward signals that focus on both energy efficiency and fairness. The RL agents can pause and resume transfer threads as needed, pausing during heavy network use and resuming when resources are available, to prevent overload and save energy. We evaluate several RL techniques and compare our solution with state-of-the-art methods by measuring computational overhead, adaptability, throughput, and energy consumption. Our experiments show up to 25% increase in throughput and up to 40% reduction in energy usage at the end systems compared to baseline methods, highlighting a fair and energy-efficient way to optimize data transfers in shared network environments.

1 Introduction

The unprecedented increase in data generated by scientific research, industrial applications, e-commerce, social networks, the Internet of Things (IoT), and emerging trends like large-scale Artificial Intelligence (AI) training workloads has created a significant demand for distributed data access, sharing, and dissemination. Consequently, global data traffic has surged exponentially, surpassing an annual rate of 5 zettabytes in 2023 [1]. To put this into perspective, this magnitude of data transfer equates to over 3 billion DVDs being shipped per day throughout the entire year over communication networks.

To meet the requirement for high-speed data movement in distributed and collaborative science projects, high-speed research networks like Internet2 [2] and ESnet [3] have been established. However, despite the availability of these high-speed networks, most data transfers achieve only a fraction of the available bandwidth due to inefficient tuning and underutilization of the available resources. There has been a considerable amount of work on network throughput optimization, proposing heuristic [4, 5, 6, 7, 8], supervised learning [9, 10, 11], and real-time optimization [12, 13, 14,

15] models to address performance limitations. While heuristic models can provide higher transfer throughput than baseline configurations, they often lack robustness in the face of dynamic network conditions. Supervised learning models, when combined with real-time probing, require extensive historical data collection under a wide range of transfer conditions, a process that can span weeks or months. Real-time optimization algorithms, although effective in finding near-optimal settings, typically suffer from long convergence times and may compromise fairness and stability in shared network environments.

Moreover, the exponential increase in data transfers has raised significant concerns over energy consumption, particularly in high-performance computing (HPC) and cloud data centers. It is estimated that information and communication technologies will consume between 8% and 21% of the world’s electricity by 2030 [16], with communication networks accounting for approximately 43% of the total IT power consumption [17]. Data transfers over the Internet now consume more than a hundred terawatt-hours of energy annually, costing around 20 billion US dollars, and recent studies even suggest that, in some scenarios, physically shipping storage media could be less carbon-intensive than network transfers [18]. Despite extensive research in power management techniques for networking infrastructure, little attention has been paid to reducing the energy consumption of the end systems (i.e., sender and receiver nodes) during active data transfers. In fact, one study shows that approximately 25% of the total electricity consumed during end-to-end data transfers occurs at the end systems on a global (intercontinental) network, a figure that increases to 60% on a nationwide network and up to 90% on a local area network [19]. Since this ratio depends on both the number of network devices (e.g., routers, switches) between sender and receiver and the power consumed by each device, decreasing end-system power consumption can lead to significant energy savings. These challenges underline the need for solutions that optimize both throughput and energy efficiency without sacrificing fairness among users in data transfer applications.

To overcome these issues, we introduce a novel deep reinforcement learning (DRL) framework, called SPARTA (Smart Parameter Adaptation via Reinforcement Learning for data Transfer Acceleration), which is built on the following key innovations:

- We train DRL agents using reward signals that are designed to balance energy consumption with fairness. This enables agents to dynamically pause and resume transfer threads based on real-time network conditions, thereby preventing resource oversaturation and reducing energy usage.
- By intelligently adjusting application-level parameters, the agents can mitigate the risk of overloading network bandwidth and CPU cores during peak times while exploiting available resources during off-peak periods. This dual adaptation not only accelerates data transfers but also maintains fairness among multiple users.
- To expedite the DRL training process, we introduce an emulation environment that leverages state transition logs captured during initial real-world training episodes. By using transitions from early episodes, our agents can efficiently learn optimal behaviors without the prohibitive time and energy costs associated with extended real data transfers.

By incorporating these innovations, SPARTA is capable of achieving substantial improvements in data transfer performance. Extensive experiments demonstrate up to 25% improvement in throughput and up to 40% reduction in energy consumption compared to baseline methods.

Compared to our previous work [20], which focused solely on tuning TCP stream counts for performance optimization, SPARTA broadens the scope by adopting a multi-parameter DRL framework that simultaneously optimizes concurrency (cc) and parallelism (p) while incorporating energy efficiency and fairness in the reward function. This comprehensive approach ensures that data transfers are not only faster but also more energy efficient and fair in shared network environments.

The rest of the paper is organized as follows: Section II provides background on the challenges of energy efficiency and fairness in high-performance network data transfers, along with related work. Section III details the design and implementation of our proposed reinforcement learning framework. Section IV presents extensive experimental evaluations of SPARTA, and Section V concludes the paper with insights and future research directions.

2 Background and Related Work

There is a considerable amount of work in the literature that tries to improve the performance of data transfers at different layers. Some work focused on developing new transport layer protocols to maximize bandwidth utilization [21, 22, 23, 24]. However, the wide adoption of a new transport layer protocol requires kernel and system modification, making this type of solution challenging. Additionally, file transfers in high-speed networks frequently encounter I/O performance constraints, enhancing congestion control algorithms alone proves insufficient to address the performance challenges present in contemporary high-performance networks.

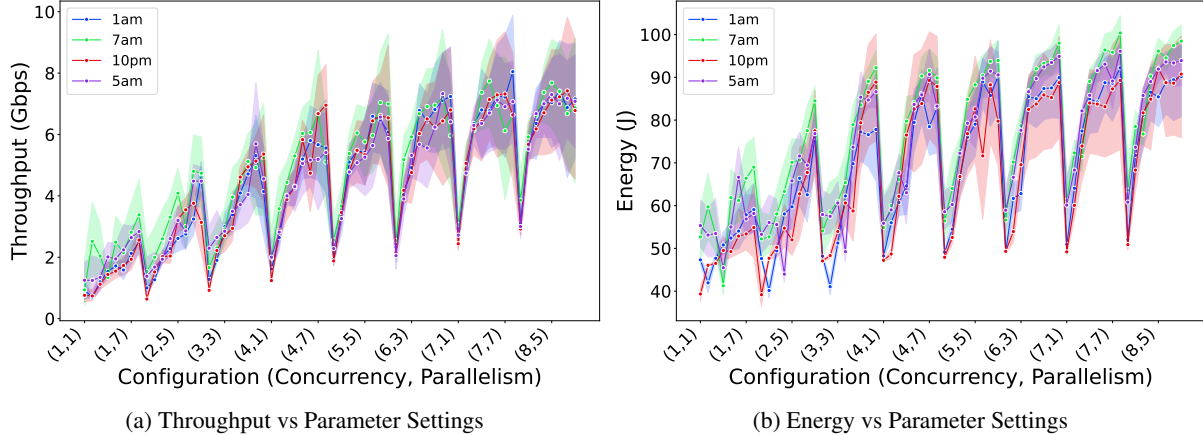


Figure 1: The plots show the throughput and energy consumption for different concurrency and parallelism settings under varying background traffic conditions observed at different times of the day in the Chameleon Cloud between TACC and UC sites, connected by a 10 Gbps network link. Subfigure (a) highlights the throughput behavior, while subfigure (b) shows the average energy consumption per measurement interval (MI) of 1 second (*power*), both influenced by the chosen levels of concurrency and parallelism. These results demonstrate the performance and energy efficiency trade-offs under different background traffic.

An effective strategy to mitigate performance issues in file transfers involves adjusting application-layer transfer parameters, including pipelining (*pp*), parallelism (*p*), concurrency (*cc*), buffer size and striping [13]. Among these parameters, parallelism and concurrency are identified as the most critical for resolving the majority of underlying performance challenges [4, 13]. *Concurrency* (*cc*) refers to task-level parallelism, where each task is the transfer of a file. By running multiple server processes or threads simultaneously, different files can be transferred at the same time, speeding up the overall transfer process. *Parallelism* (*p*) denotes the number of parallel streams for each file transfer process or thread. It is beneficial for transferring medium sized and large files. Increasing the total number of data streams ($cc \times p$) can enhance the transfer throughput. However, excessive use can lead to network congestion and trigger TCP’s congestion avoidance algorithm, reducing the sending rate. When meticulously optimized, these parameters can substantially enhance end-to-end data transfer performance by addressing common bottlenecks such as inadequate I/O parallelism and TCP buffer size limitations [20].

Previous research has explored various methods for tuning application-layer parameters, focusing on maximizing throughput. *Heuristic-based* systems [4, 5, 6, 7, 8] often outperform simple single-stream baselines but do not adapt well to changing network conditions (e.g., varying background traffic in different networks). *Supervised learning* approaches [9, 10, 11] leverage historical data to predict optimal parameter settings. However, gathering large, representative datasets under diverse transfer conditions can be time-intensive and expensive. *Online methods* [12, 13, 15] continuously adjust parameters but may experience lengthy convergence times and lack fairness safeguards in multi-tenant environments.

A popular data transfer solution, Globus [25], uses static concurrency (2–8) and does not respond to changing network conditions, often underutilizing available bandwidth. ProbData [26] applies stochastic approximation to tune parameters but can require hours to converge, while PCP [13] relies on hill-climbing in a reduced search space, limiting speed and precision. Some earlier work [4, 11] employed heuristic and historical-data models to estimate parameter settings that maximize throughput; however, such solutions depend on extensive historical logs from production networks. In many cases, the cost and complexity of assembling these logs renders them impractical.

There has been also some prior work on energy-efficient data transfer optimization. Most existing work in this area has centered on reducing power usage within the network core (e.g., switches and routers) [27, 28, 29, 30, 31, 32, 33, 34, 35, 36, 37, 38, 39, 40, 41]. While these approaches reduce overall network energy consumption, they can also degrade performance (e.g., by putting idle components to sleep) or require costly hardware replacements, limiting their practicality in the short term.

By comparison, fewer studies address energy use in end-to-end data transfers, particularly emissions at the sender and receiver systems during active transfers. Existing methods—ranging from heuristic-based [42, 5, 43] to historical-data-driven [10, 9]—typically focus on adjusting transfer parameters while honoring throughput or energy targets specified by service-level agreements (SLAs). However, building robust historical models demands extensive data covering diverse traffic conditions, which is both time-consuming and costly, and heuristics tend to falter when applied to new or different network settings.

3 Model Overview

3.1 Why Reinforcement Learning?

Existing heuristic solutions cannot easily adapt to the dynamic nature of wide-area networks, where optimal concurrency (cc) and parallelism (p) depend on both static factors (e.g., hardware limits, available network bandwidth) and highly variable conditions (e.g., background traffic, transient congestion). Figure 1 displays throughput and energy consumption for various concurrency and parallelism settings under different network traffic conditions in the Chameleon Cloud [44] between TACC and UC sites. These sites are connected by a 10 Gbps network, and the experiment involved transferring 50 files of 1 GB each using TCP CUBIC [45]. The plots illustrate how varying the levels of cc and p influences receiver-side throughput and energy usage. The results highlight the trade-offs between performance and energy efficiency under various network conditions. The relationship between the parameters is non-linear, and the optimal settings can improve performance by up to 10 times compared to baseline settings (where concurrency (cc) = 1 and parallelism (p) = 1). As background traffic changes, the optimal settings for throughput and energy also shift. With limited network signals available from end hosts, an ideal data transfer solution needs to adjust cc and p to maintain optimal performance and energy consumption.

To understand why an adaptable solution is required, we consider the well-known models for single- and multi-stream TCP throughput. In this study, we analyze loss-based TCP variants, such as TCP CUBIC [45], for all our analysis. When the packet loss ratio $L < 1\%$, a single TCP flow’s throughput can be approximated as [46]:

$$TCP_{thr} \leq \frac{MSS}{RTT} \cdot \frac{C}{\sqrt{L}}, \quad (1)$$

where MSS is the maximum segment size, RTT is the round-trip time, C is a constant factor, and L is the packet loss ratio. For n parallel TCP streams, the aggregate throughput can be approximated by summing each flow’s bandwidth [47]:

$$TCP_{agg} \leq \frac{C}{RTT} \left[\frac{MSS}{\sqrt{L_1}} + \dots + \frac{MSS}{\sqrt{L_n}} \right]. \quad (2)$$

While adding parallel streams can boost throughput by effectively enlarging a “virtual” MSS , the benefits vanish if packet loss rises from congestion or if the bottleneck link is fully saturated. Consequently, an optimal stream count exists that maximizes throughput without triggering excess loss. However, due to fluctuating background traffic, this “optimal” stream count varies throughout the transfer session and across different network paths.

Heuristic methods for fixed or slowly adapting concurrency and parallelism struggle in dynamic environments. We need a framework that: (1) requires no prior knowledge of the network or endpoints, (2) derives insights solely from local observations (e.g., throughput, RTT, packet loss) available at end hosts, (3) learns the mapping between these signals and the current network congestion state, and (4) handles partial observability (i.e., incomplete visibility of network internals).

Reinforcement Learning (RL), especially Deep Reinforcement Learning (DRL), fulfills these criteria by treating concurrency (cc) and parallelism (p) parameter selection as a sequential decision-making problem. The agent observes performance signals (e.g., RTT and its derivatives, packet loss rate), takes an action (e.g., increasing/decreasing cc or p), and receives a reward that encodes its objectives (e.g., higher throughput, lower energy usage, or fairness).

Because network congestion states are not fully observable from the end host, the agent’s policy function approximator infers hidden conditions by continuously monitoring above mentioned feedback signals as state. Over time, the DRL algorithm discovers the “sweet spot” for concurrency and parallelism level at any given instant, dynamically reacting to background traffic changes.

3.2 Optimization Goals and Problem Formulation

Our novel solution, SPARTA, provides a flexible way to optimize different objectives by adjusting the reward function during training. It aims to maximize data throughput while either (1) promoting fairness and indirectly reducing energy via low congestion, or (2) prioritizing throughput per unit energy.

3.2.1 Fairness and Efficiency Objective

A key aim in shared networks is to achieve high throughput without disproportionately harming other transfers sharing the link. We adopt a utility function $U(T, L)$ [15] that rewards higher throughput T and penalizes loss L :

$$U(T, L) = \frac{T}{K^{(cc \times p)}} - T \cdot L \cdot B, \quad (3)$$

where K and B are constants controlling the relative weight of throughput scaling and the cost of loss. By discouraging congestion (i.e., excessive packet loss), this objective not only ensures fairness but also reduces retransmissions and idle waiting, indirectly improving energy efficiency.

The goal is to choose concurrency (cc) and parallelism (p) that maximize the cumulative utility between transfer start time t_s and finish time t_f :

$$\begin{aligned} \operatorname{argmax}_{\{cc,p\}} \quad & \sum_{t=t_s}^{t_f} U(T_t, L_t) \\ \text{subject to:} \quad & cc \times p \leq \mathbb{N}_{\text{streams}}, \\ & T_t \leq b, \end{aligned} \quad (4)$$

where T_t and L_t are the throughput and packet loss rate at interval t , and b is the link capacity. By avoiding congestion, the agent prevents wasted energy from retransmissions and queuing delays, thereby promoting both fairness and efficiency.

3.2.2 Throughput-Focused Energy Objective

Some applications prioritize minimizing energy consumption while still achieving acceptable throughput. To address this, we use the throughput-to-energy ratio $\frac{T_t}{E_t}$ at each interval t , where T_t is the throughput and E_t is the energy consumption:

$$\begin{aligned} \operatorname{argmax}_{\{cc,p\}} \quad & \sum_{t=t_s}^{t_f} \frac{T_t}{E_t} \\ \text{subject to:} \quad & cc \times p \leq \mathbb{N}_{\text{streams}}, \\ & T_t \leq b, \end{aligned} \quad (5)$$

where b is the available bandwidth. This formulation explicitly rewards higher throughput per unit of energy, making it especially relevant in energy-constrained environments.

3.2.3 Adaptive DRL Framework and Interrelation of Objectives

Both the fairness-and-efficiency (Eq. 4) and throughput-focused energy (Eq. 5) objectives can be integrated into the same DRL framework via a customizable reward:

$$r_t = \begin{cases} U(T_t, L_t), & \text{(Fairness \& Efficiency)} \\ \frac{T_t}{E_t}, & \text{(Throughput-Focused Energy)} \end{cases} \quad (6)$$

By penalizing loss, the first reward indirectly lowers energy overhead through congestion avoidance, while the second directly optimizes throughput per unit energy. In practice, either reward can be selected based on deployment needs, allowing SPARTA to accommodate diverse operational goals and constraints.

3.3 DRL State Space, Actions and Reward

3.3.1 DRL State Space

Designing an effective state space requires focusing on features that reliably indicate network conditions without directly including the performance metrics (e.g., throughput, energy) the agent aims to optimize. This separation ensures the agent learns the relationship between its actions and these metrics indirectly, yielding more robust, generalizable policies. Rather than using raw, highly variable measurements, we extract more stable indicators at each Monitoring Interval (MI), for instance:

- *RTT* gradient: Reflects how *RTT* changes over time rather than its instantaneous value.
- *RTT* ratio [48]: Compares the current mean *RTT* to the minimum observed mean *RTT* since the start of the session, normalizing against the session's best performance.

- Packet loss rate (plr): Highlights network congestion more directly than throughput or energy values, which are the final optimization targets.

The agent’s controllable settings—concurrency (cc) and parallelism (p)—are also included in the state, enabling the RL algorithm to learn how past parameter choices affect the current network state.

To capture temporal dynamics, we store n consecutive observations (one per MI). Let x_t be the signal vector at time t :

$$x_t = \{plr_t, rtt_gradient_t, rtt_ratio_t, cc_t, p_t\}. \quad (7)$$

Then the state s_t is:

$$s_t = (x_{t-n}, \dots, x_{t-1}, x_t), \quad (8)$$

allowing the agent to detect trends in plr , RTT metrics, and parameter updates over the last n intervals.

By tracking these features over time, the agent learns how past adjustments to (cc, p) influence future network conditions, discovering how to indirectly maximize throughput and minimize energy consumption. In essence, this state design balances simplicity and expressiveness, helping the RL approach adapt effectively to real-world, dynamically changing networks.

3.3.2 Action Space and Parameter Constraints

All the DRL algorithms we evaluate – on-policy (PPO [49], R_PPO [50]) and off-policy (DDPG [51], DQN [52], DRQN [53]) – use a discrete action space of five actions that jointly modify concurrency (cc) and parallelism (p). At each monitoring interval (MI) t , the agent picks an action $a_t \in \{0, 1, 2, 3, 4\}$, which updates (cc_{t+1}, p_{t+1}) as follows:

$$\begin{aligned} a_t = 0 &\rightarrow (cc_{t+1}, p_{t+1}) = (cc_t, p_t) \\ a_t = 1 &\rightarrow (cc_{t+1}, p_{t+1}) = (cc_t + 1, p_t + 1) \\ a_t = 2 &\rightarrow (cc_{t+1}, p_{t+1}) = (cc_t - 1, p_t - 1) \\ a_t = 3 &\rightarrow (cc_{t+1}, p_{t+1}) = (cc_t + 2, p_t + 2) \\ a_t = 4 &\rightarrow (cc_{t+1}, p_{t+1}) = (cc_t - 2, p_t - 2) \end{aligned}$$

In methods like PPO, R_PPO, and DDPG, the policy can internally produce separate real-valued outputs for cc and p (e.g., $(x_1, x_2) \in \mathbb{R}^2$), which are then floored or capped to map them into one of the five discrete actions. This approach supports finer control over concurrency and parallelism, yet still converges on the same discrete final choice.

We start with predefined (cc_0, p_0) (e.g., $(4, 4)$), derived from prior logs or experience, to avoid random extremes. Additionally, we enforce:

$$cc_{\min} \leq cc_t \leq cc_{\max} \quad \text{and} \quad p_{\min} \leq p_t \leq p_{\max}, \quad (9)$$

clipping any actions that would exceed these limits. By bounding concurrency and parallelism in this way, we avoid overloading the network and end hosts while ensuring performance remains above a minimum baseline.

Although each DRL algorithm handles exploration differently (e.g., continuous outputs vs. discrete Q-tables), all converge on the same five discrete updates. This uniform action design simplifies comparisons across algorithms and ensures a clear mapping between each algorithm’s decisions and the concurrency (cc) and parallelism (p) configuration. Overall, this setup allows the agent to explore concurrency and parallelism in a controlled manner, preserving system stability and enabling effective parameter tuning.

3.3.3 Reward Formulation under Different Objectives

Our DRL agent’s reward function r_t is designed to steer learning toward specific performance objectives. We primarily consider two reward formulations—one that promotes both fairness and efficiency (by reducing congestion and indirectly saving energy), and another that explicitly targets throughput per unit energy. This framework can be extended to additional objectives by tailoring the reward function.

Fairness and Efficiency Reward:

This reward is based on the utility function $U(T, L)$ (see Section 3.2), which rewards higher throughput T while penalizing higher packet loss L . By discouraging congestion (i.e., high loss), this objective not only promotes fair bandwidth sharing but also indirectly reduces energy wasted on retransmissions and idle waiting:

$$U(T, L) = \frac{T}{K^{(cc \times p)}} - T \cdot L \cdot B, \quad (10)$$

For each measurement interval, the agent computes utility values $\{U_{t-n+1}, \dots, U_t\}$ and forms an average:

$$\bar{U}_t = \frac{1}{n} \sum_{i=t-n+1}^t U_i. \quad (11)$$

The reward is then defined as:

$$r_t = f(\bar{U}_t, r_{t-1}), \quad (12)$$

where $f(\cdot)$ measures the improvement relative to a rolling baseline.

Throughput-Focused Energy Efficiency Reward:

For energy-sensitive environments, the reward is defined based on throughput achieved per unit energy consumed. During each MI, let T_i denote the throughput and E_i the energy consumption. We compute:

$$\bar{T}_t = \frac{1}{n} \sum_{i=t-n+1}^t T_i, \quad \text{and} \quad \bar{E}_t = \max_{i \in [t-n+1, t]} E_i, \quad (13)$$

which yields an energy efficiency metric:

$$\bar{R}_t = \frac{\bar{T}_t \cdot SC}{\bar{E}_t}, \quad (14)$$

where SC is a scaling constant. The corresponding reward is given by:

$$r_t = f(\bar{R}_t, r_{t-1}). \quad (15)$$

This formulation explicitly incentivizes higher throughput per unit energy, aligning with energy-constrained operation.

Difference-Based Reward Update ($f(\cdot)$):

A practical choice for $f(\cdot)$ leverages the difference between consecutive rewards to encourage incremental improvements. Specifically, let r_t be the current metric (either \bar{U}_t or \bar{R}_t) and r_{t-1} be the previous one. We define:

- $f(r_t, r_{t-1}) = x$, if $r_t - r_{t-1} > \epsilon$,
- $f(r_t, r_{t-1}) = y$, if $r_t - r_{t-1} < -\epsilon$,
- $f(r_t, r_{t-1}) = 0$, otherwise,

where x and y are positive and negative rewards, respectively, and ϵ controls sensitivity. If ϵ is too small, the agent may oscillate due to frequent reward changes; if it is too large, learning may slow as only substantial improvements trigger non-zero rewards.

3.3.4 Unified DRL Optimization Problem

Regardless of the chosen DRL algorithm (PPO, R_PPO, DDPG, DQN, or DRQN) and the specific action space configuration, the agent aims to maximize the expected sum of discounted rewards:

$$\operatorname{argmax}_{\theta} \mathbb{E} \left[\sum_{t=t_s}^{t_f} \gamma^{t-t_s} r_t \right], \quad (16)$$

where $\gamma \in (0, 1]$ is the discount factor and r_t is defined according to the selected performance objective. On-policy methods (PPO, R_PPO) estimate the policy gradient using samples drawn from the current policy, while off-policy methods (DDPG, DQN, DRQN) leverage replay buffers or target networks. The selected action space representation and reward function define the agent's experience and, ultimately, its learned policy.

By appropriately choosing the action space structure and the reward function, we ensure that the agent can adapt to different optimization goals (fairness or energy efficiency), handle various RL algorithms, and dynamically learn to set optimal concurrency and parallelism parameters.

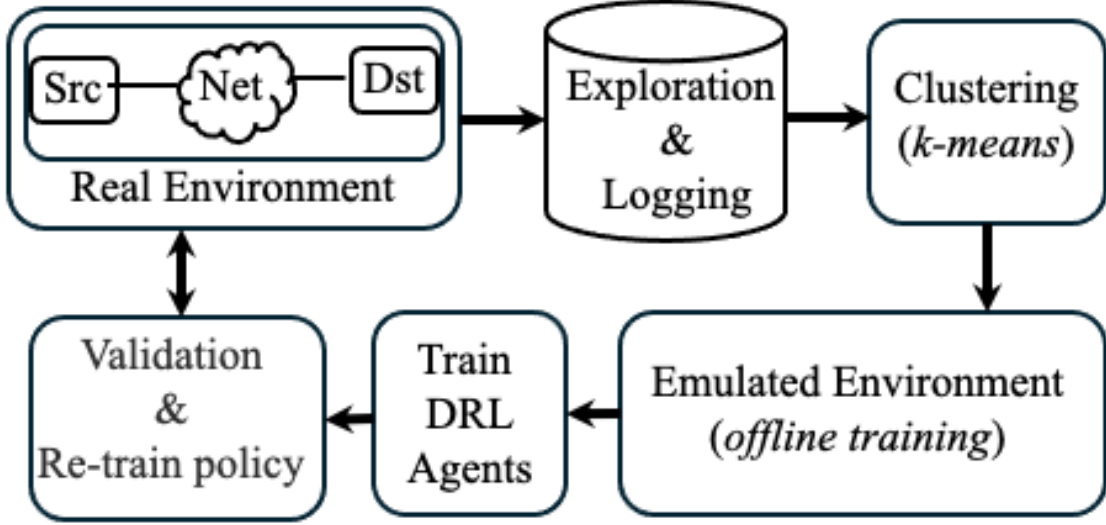


Figure 2: Overview of the offline-online training process, which involves a real environment where data is collected from the source (Src) through the network (Net) to the destination (Dst). The collected data undergoes exploration and logging, followed by clustering using k -means. The resulting data is used for training DRL agents in an emulated environment, with a feedback loop for validation and re-training of the policy.

3.4 Emulated Training Environment

To accelerate the DRL agent’s learning and minimize the time and energy costs associated with suboptimal data transfers, we built an emulated training environment from previously recorded *state-action transitions* and instantaneous transfer metrics. Traditional online training requires continuous interactions with a real system, causing many low-efficiency transfers before reaching a near-optimal policy. In contrast, our emulated setup refines the agent’s decision-making *offline*, reusing previously observed transitions to approximate real-world dynamics without repeatedly incurring inefficient runs. Figure 2 summarizes this offline-online process.

First, we deploy the DRL agent in a real environment under a high-exploration regime. During this phase, each second of the Monitoring Interval (MI) generates a transition log, recording instantaneous metrics such as throughput, loss rate (plr), round-trip time (RTT), energy consumption, and current (cc, p). Each entry also includes a *utility score* derived from the chosen reward function. An illustrative entry might be:

- 1707718539.468927 -- INFO:
 Throughput:8.32Gbps
 lossRate:0
 parallelism:7
 concurrency:7
 score:3.0
 rtt:34.6ms
 energy:80.0J

These per-second transitions form the backbone of the emulation. Each line effectively encodes (state, action, next_state), where, **state** is the features extracted from previous MIs (e.g., plr , $rtt_gradient$, rtt_ratio , current (cc, p)); **action** is the discrete choice (e.g., increase/decrease cc and p); and **next state and performance** is the resulting per-second throughput, plr , RTT, and energy consumption following the agent’s action. After sufficient exploratory runs, we accumulate transitions from a wide array of network conditions.

To structure these transitions, we convert each second’s measurements (e.g., throughput, RTT, plr , (cc, p)) into a feature vector:

$$x = [plr, rtt_gradient, rtt_ratio, cc, p] \quad (17)$$

Hence, each transition becomes (x_t, a_t, x_{t+1}, U_t), where U_t denotes the utility score. We then apply a clustering algorithm, such as k -means [54], grouping transitions that share similar features and outcomes. Each cluster’s centroid represents a recurring “network scenario,” enabling a simplified lookup when simulating new training episodes.

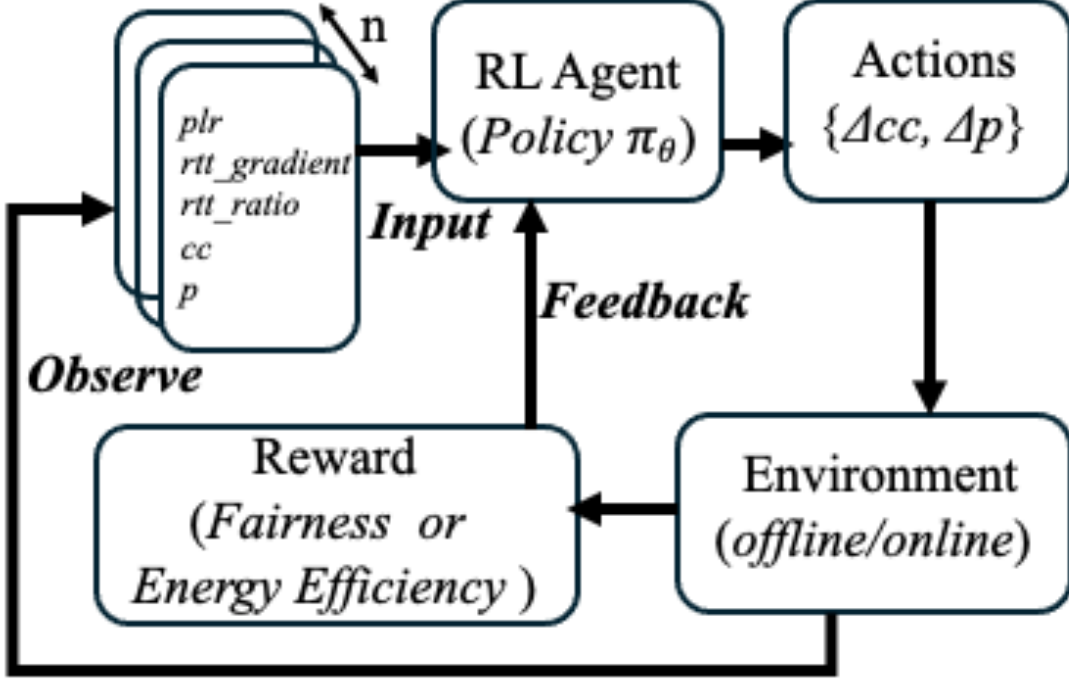


Figure 3: Diagram illustrates the primary DRL components for optimizing transfer parameters. The agent observes the state features (e.g., plr , $rtt_gradient$, rtt_ratio , cc , p), takes an action ($\{\Delta cc, \Delta p\}$), and receives a reward based on fairness or energy-efficiency objectives, all within an environment.

Once clustered, our emulator acts as a *lookup-based* environment:

1. *Initialization*: Randomly pick an initial state (cc_0, p_0) from the dataset for the start of a training episode.
2. *Action Selection*: Whenever the DRL agent chooses an action a_t , identify the cluster whose centroid most closely matches (x_t, a_t) .
3. *Uniform Sampling*: Randomly select a transition from the matching cluster to produce x_{t+1} and the associated throughput, loss, and energy. This step simulates what might happen in a real transfer, without performing another physical run.

Each cluster contains multiple similar transitions, introducing beneficial variability into the next state and preventing overfitting to a single deterministic mapping.

Suppose the emulator’s current x_t features $(cc, p) = (7, 7)$ under low-loss conditions, and the agent selects action $a_t = 1$ (i.e., increment both concurrency and parallelism by one). Concretely, this translates to $(cc_t, p_t) = (7, 7) \rightarrow (8, 8)$. We then search for a cluster whose centroid matches (x_t, a_t) , meaning a scenario transitioning from $(7, 7)$ to $(8, 8)$. Assume we find Cluster 1, containing transitions that achieved, say, 8.96 Gbps at moderate additional energy cost. We uniformly sample a transition from Cluster 1 and return the next state with updated throughput and energy metrics—without re-running an actual transfer. By repeatedly interacting with this emulator, the DRL agent hones its policy offline, yielding faster convergence and lower real-world resource consumption compared to purely online learning.

Once the agent demonstrates strong performance in the emulator, we validate and, if necessary, re-train it in the real environment (see Figure 2). This iterative offline-online process keeps training costs low while preserving real-world accuracy; any newly gathered transitions can be clustered and added to the emulator, ensuring it remains up-to-date with evolving network states.

3.5 Evaluated DRL Algorithms

In this work, we consider a variety of DRL algorithms to handle the complex problem of optimizing concurrency (cc) and parallelism (p) under varying network conditions. Figure 3 illustrates how the agent observes recent states and selects actions to adjust cc and p , receiving rewards (e.g., fairness or energy efficiency) from the environment.

We evaluate both on-policy and off-policy algorithms to ensure that our approach is robust across different training paradigms. In particular, the five algorithms—DQN, DRQN, PPO, R_PPO, and DDPG—were chosen as representative methods for their unique strengths: DQN for its simplicity; DRQN and R_PPO for handling the partially observable network state via recurrent structures that capture patterns from state history; and PPO and DDPG as examples of on-policy and off-policy approaches, respectively, covering a broad spectrum of reinforcement learning strategies.

Deep Q-Networks (DQN) [52] combine Q-learning with deep neural networks, enabling the agent to approximate Q-values for high-dimensional state spaces. We construct a state vector by concatenating a fixed number of recent state observations, allowing the network to capture short-term temporal patterns. While effective for many tasks, DQN struggles with continuous actions and partially observable environments. Its simplicity makes it a useful baseline for our evaluation.

Proximal Policy Optimization (PPO) [49] is a policy gradient method that adjusts the policy parameters to improve performance while constraining large updates. Similar to DQN, we represent the state as a concatenation of recent observations. PPO’s clipping mechanism ensures stable and efficient learning, making it suitable for continuous or discrete actions. As an on-policy method, it complements the off-policy approaches and provides insights into the benefits of policy gradient methods for our problem.

Deep Deterministic Policy Gradient (DDPG) [51] is designed for continuous action spaces. It uses actor-critic architectures, where the actor outputs deterministic actions and the critic estimates Q-values. As with DQN and PPO, we feed a concatenated state vector to both actor and critic networks. DDPG represents the off-policy continuous control paradigm, making it an important candidate for optimizing the fine-grained adjustments required in network tuning.

Recurrent PPO (R_PPO) extends PPO by incorporating recurrent neural network layers (e.g., LSTMs) to handle partial observability and longer-term dependencies in the data [55, 50]. Instead of concatenating multiple states into a single vector, a window of past states is passed through the recurrent structure, enabling the agent to maintain an internal memory of historical network conditions and better adapt to fluctuating environments. This recurrent formulation is crucial for capturing the temporal patterns in network performance metrics.

Deep Recurrent Q-Networks (DRQN) [53] augment DQN with recurrent units, allowing the agent to handle partially observable scenarios by storing information over time. Similar to R_PPO, the DRQN agent receives a window of states, feeding them sequentially into its recurrent layer. This approach provides temporal context and improves decision-making when immediate observations are insufficient.

By evaluating these algorithms, we determine which DRL method best captures the temporal dynamics, handles partial observability, and effectively optimizes throughput and energy consumption. The inclusion of both on-policy and off-policy methods, as well as models with and without recurrent architectures, ensures a comprehensive assessment of DRL techniques.

This high-level procedure (inspired by the reinforcement learning frameworks described in algorithm 1 outlines how various DRL models are trained to adjust concurrency (cc) and parallelism (p) in dynamic network environments.

- **Lines 1–2: Initialization.** The agent and environment are set up according to the chosen RL model (DQN, DRQN, PPO, R_PPO, or DDPG). The model parameters (e.g., neural network weights) are randomly initialized, and an experience buffer (for off-policy methods) is prepared.
- **Lines 3–4: Outer Training Loop.** The algorithm runs for a predefined number of episodes N , resetting the environment at the start of each episode.
- **Lines 5–10: Per-Step Operations.** At each time step, the agent observes the current state (e.g., history of plr , $rtt_gradient$, rtt_ratio , cc , p), selects an action (increment or decrement cc and p), applies it to the environment, and receives a reward reflecting the objective (fairness or energy efficiency).
- **Lines 11–12: Storage and Update.** The agent stores the transition (s_t, a_t, r_t, s_{t+1}) in either a replay buffer (off-policy) or a trajectory buffer (on-policy) and updates its policy or Q-value function using one of the RL optimization methods. This step leverages the well-known gradient-based updates [52, 49, 51] to minimize loss functions or maximize clipped surrogate objectives.
- **Lines 13–14: Termination Condition.** Each episode ends when the agent reaches the final time step T or when an environment-defined terminal state occurs (e.g., completion of a transfer or a set of transfer intervals).
- **Final Return.** After N episodes, the algorithm produces a trained policy π_θ (and possibly a learned value function V_ψ or Q-function Q_ψ), which can then be used to select cc and p in real or emulated network environments.

Algorithm 1: SPARTA Training Procedure**Require: Models:** A chosen DRL model from $\{DQN, DRQN, PPO, R_PPO, DDPG\}$;**Environment:** Provides states s , actions a , and rewards r **Hyperparameters:** Learning rate, discount factor γ , exploration rate, etc.**Ensure:** A trained policy $\pi_\theta(a | s)$ (and possibly a value function $V_\psi(s)$ or $Q_\psi(s, a)$) for optimizing concurrency (cc) and parallelism (p)1: **Initialize** model parameters (e.g., θ, ψ for actor-critic), set replay buffer \mathcal{D} empty for off-policy methods2: Define maximum number of training episodes N and per-episode length T 3: **for** episode = 1 to N **do**4: Reset environment and obtain initial state s_1 5: **for** $t = 1$ to T **do**6: **Observe current state** s_t (e.g., $plr, rtt_gradient, rtt_ratio, cc, p$)7: **Select action** a_t according to the DRL method:• **On-policy** (PPO, R_PPO): sample $a_t \sim \pi_\theta(a | s_t)$ • **Off-policy** ($DQN, DRQN, DDPG$):- **DQN/DRQN:** ϵ -greedy over $Q_\psi(s_t, a)$ - **DDPG:** $a_t = \pi_\theta(s_t) + \text{noise}$ 8: Execute a_t in the environment to get new state s_{t+1} and reward r_t 9: **Store transition** (s_t, a_t, r_t, s_{t+1}) :• For **off-policy** methods, place in replay buffer \mathcal{D} • For **on-policy** methods, store in the current trajectory10: **Update model parameters** (frequency-dependent):• **DQN/DRQN:** sample mini-batches from \mathcal{D} to minimize:

$$(Q_\psi(s, a) - [r + \gamma \max_{a'} Q_\psi(s_{t+1}, a')])^2$$

• **DDPG:** sample mini-batches from \mathcal{D} to update critic:

$$y_t = r + \gamma Q_\psi(s_{t+1}, \pi_\theta(s_{t+1}))$$

and use policy gradient to update the actor

• **PPO/R_PPO:** after collecting a rollout, optimize clipped surrogate objective:

$$\mathcal{L}_\pi = \mathbb{E}_t [\min(r_t(\theta) \cdot A_t, \text{clip}(r_t(\theta), 1 - \epsilon, 1 + \epsilon) \cdot A_t)]$$

11: **if** end of episode or environment termination **then**12: **break**13: **end if**14: **end for**15: **end for**16: **return** policy π_θ (and Q_ψ or V_ψ if applicable).

Method	Offline Training Time (min) ↓	Steps in Converging ↓	Training Avg CPU% ↓	Training Avg GPU% ↓	Training Avg Memory% ↓	Training Avg Energy(KJ) ↓	Inference Time (ms) ↓	Model Inference Energy (J) ↓	Energy During Online Tuning (KJ) ↓
DQN	30	300K	26.62	10.8	16.74	131	0.57	0.098	4.3
PPO	36	600K	26.31	11.71	16.75	158	0.74	0.088	2.6
DDPG	59	320K	26.11	25.59	20.74	294	0.58	0.091	9.18
R_PPO	48.5	550K	26.93	15.41	19.27	221	0.66	0.094	4.01
DRQN	94	400K	26.67	12.67	17.66	214	0.21	0.088	5.35

Table 1: Comparison of RL algorithms trained for 100000 steps with associated training metrics.

3.6 Comparison of DRL Solutions

This section presents the comparison of five DRL algorithms (DQN, PPO, DDPG, R_PPO, and DRQN) for throughput focused energy objective (T/E) of data transfer optimization. We begin with a brief overview of the setup for offline training, followed by an analysis of the metrics in Table 1. Finally, we discuss the throughput and energy performance in both simulation and real-world transfers.

3.6.1 Offline Training Setup

To facilitate offline training, we first gathered transition data from a real-world environment (Chameleon Cloud, TACC to UC), with a wide range of cc and p settings. These transitions, logged at per-second intervals, captured throughput, packet loss rate (plr), round-trip time (RTT), and energy usage. By including both suboptimal and near-optimal parameter combinations, the dataset covered diverse network conditions (e.g., congestion levels, and background load). Each transition comprised a state (featuring $plr, rtt_gradient, rtt_ratio, cc, p$), an action (changes to cc and p), and the resulting throughput and energy. We then employed clustering-based emulation (Section 3.4) to train each DRL model without repeatedly interacting with the real network, achieving more efficient policy convergence.

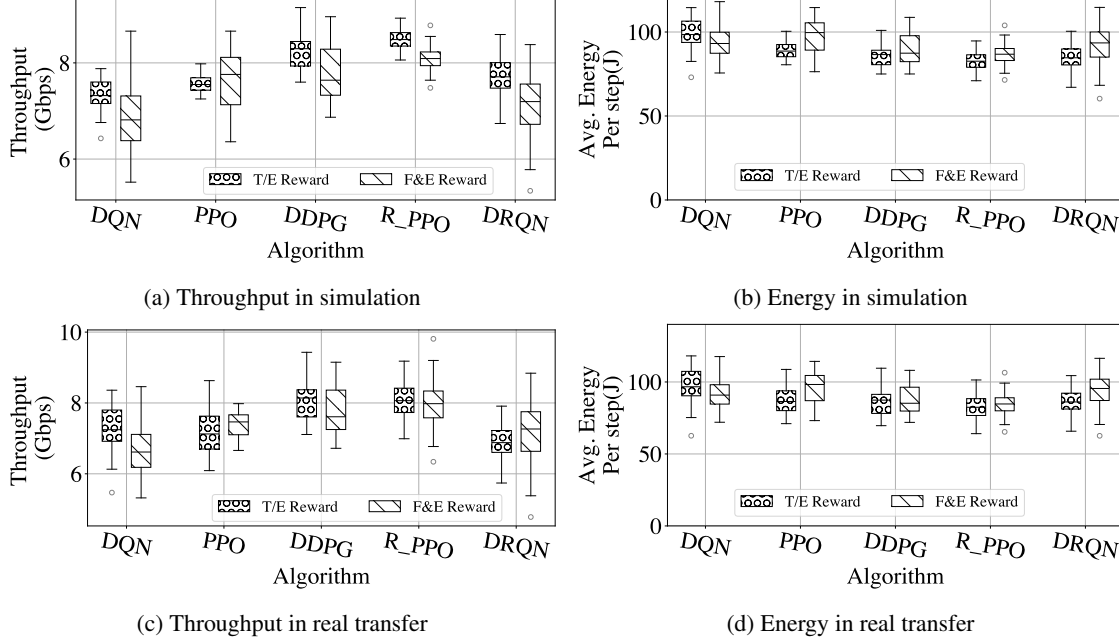


Figure 4: Comparison of Various DRL Algorithms trained on offline historical data using F&E Reward (Fairness and Efficiency Reward) and T/E Reward (Throughput-Focused Energy Efficiency Reward), and evaluated in simulation and real-world transfers between Chameleon Cloud (TACC) and UC sites.

3.6.2 Analysis of Results in Table 1

Table 1 compares five DRL algorithms across several metrics:

Offline Training Time (min) ↓ and Steps in Converging ↓: These columns show the duration (wall-clock minutes) and interaction steps required for each method to reach a stable policy in *offline* mode. For example, DQN converges fastest (30 minutes, 300K steps), while DRQN is slowest (94 minutes), likely due to its recurrent architecture and additional computation needed to handle partial observability.

Offline Training Avg CPU% ↓, Offline Training Avg GPU% ↓, Offline Training Avg Memory% ↓: These columns detail resource usage during the offline phase. DDPG exhibits the highest GPU load (25.59%), suggesting its larger batch sizes and actor-critic updates are more GPU-intensive. By contrast, DQN and PPO show moderate GPU usage. DRQN’s recurrent layers keep CPU utilization comparable but slightly increase memory consumption.

Offline Training Energy (KJ) ↓: This metric captures the total energy consumption over the offline training run. DQN uses the least energy (131 KJ) to converge, whereas DDPG expends the most (294 KJ), aligning with its longer training horizon and heavier GPU load.

Inference Time (ms) ↓ and Model Inference Energy (J) ↓: After training, each model’s *per-step* inference cost is measured. DQN has an inference time of 0.57 ms and about 0.098 J per step. DRQN, a lower mean inference time (0.21 ms), consumes around 0.088 J. PPO, being policy-gradient, has a slower inference time (0.74 ms) but also shows the lowest per-inference energy at 0.088 J.

Energy During Online Tuning (KJ) ↓: When the agent must adapt to new conditions in a real world setting, this column indicates how much additional energy is required for ongoing learning. PPO displays the smallest overhead (2.6 KJ), while DDPG’s overhead is notably higher (9.18 KJ).

Overall, these findings illustrate each algorithm’s trade-offs in training speed, resource usage, and energy efficiency, providing a basis for selecting the method that best aligns with specific performance and operational requirements.

3.6.3 Performance in Throughput and Energy

Figure 4 compares throughput and energy usage for each DRL algorithm, with the top row showing simulation results and the bottom row showing real-world transfers between TACC and UC sites of Chameleon cloud.

In simulation, DQN achieves moderate throughput (around 6–7.5 Gbps) alongside relatively low energy consumption, suggesting partial generalization from offline data. DDPG often pushes throughput closer to 8 Gbps but at a higher energy cost. PPO provides stable performance near 7 Gbps, striking a balanced trade-off between speed and energy overhead. Its recurrent variant, R_PPO, adapts more effectively to fluctuating conditions, often matching or slightly exceeding PPO’s median throughput while remaining energy-competitive. DRQN likewise benefits from recurrent memory but can incur higher energy usage in some runs, reflecting incomplete generalization.

Under real-world conditions as shown in figure 4c and 4d, these trends observed in simulation persist with additional variance. DDPG continues to seek higher throughput but at a notable energy penalty, while DQN and PPO maintain lower overall throughput and energy use. R_PPO stands out for quickly adjusting concurrency and parallelism, often sustaining consistent throughput in dynamic network conditions. DRQN’s performance improves but still shows episodes of increased energy cost. Overall, each algorithm exhibits a unique throughput–energy balance; where one underperforms, it often indicates that the model has not fully generalized from offline to real network states.

3.6.4 Online Tuning Performance and Final Selection

Figure 5 shows the cumulative reward over 500 episodes when agents—trained on Chameleon nodes for throughput focused energy objective (T/E)—are deployed to CloudLab nodes. Early on, all algorithms see a dip in performance due to the new environment’s distinct RTT patterns and congestion levels. Over time, most agents adapt, but their final reward levels vary, indicating different degrees of generalization:

- DQN and DDPG initially underperform and display larger fluctuations. Although they improve with more episodes, their cumulative rewards remain lower on average.
- PPO adapts more smoothly, maintaining a higher reward than DQN and DDPG. Its on-policy updates help it generalize, but it takes longer to match its prior performance.
- R_PPO stands out for quickly reaching a higher reward plateau, reflecting both on-policy stability and recurrent memory that better handles the new network’s partial observability. By episode 200, R_PPO has already surpassed the other algorithms, indicating stronger generalization.

Overall, these tuning trajectories highlight that agents not fully tailored to the new environment can struggle to achieve higher rewards, whereas PPO- and especially R_PPO-based policies exhibit more robust adaptation and faster convergence under different network conditions.

3.6.5 Why R_PPO for SPARTA? Training and Inference Cost Analysis

While Table 1 shows that R_PPO has higher training and inference overhead compared to some other algorithms (e.g., DQN or PPO), Figures 4 and 5 highlight its superior transfer performance (higher throughput and/or lower energy during actual data movement). This trade-off can be captured mathematically by examining the total energy cost associated with both training and inference.

Let $E_{\text{train}}(M)$ be the energy (in KJ) required to train model M , and $E_{\text{inf}}(M)$ be the energy (in J) consumed per inference step. For a given data-transfer job that requires S inference steps (e.g., S monitoring intervals) and for T total jobs, the overall cost to use model M is:

$$\text{TotalCost}(M) = E_{\text{train}}(M) + T \times S \times E_{\text{inf}}(M).$$

We define the *average overhead* per transfer as:

$$\bar{O}(M) = \frac{\text{TotalCost}(M)}{T} = \frac{E_{\text{train}}(M)}{T} + S \times E_{\text{inf}}(M).$$

As T grows large (i.e., the algorithm is used repeatedly in production), the training cost $\frac{E_{\text{train}}(M)}{T}$ is amortized over many transfers, and the main factor becomes the per-inference cost $E_{\text{inf}}(M)$. Hence, if R_PPO consistently achieves better throughput or lower transfer energy than other algorithms, its higher upfront training cost will be offset once it is used for a sufficient number of transfers.

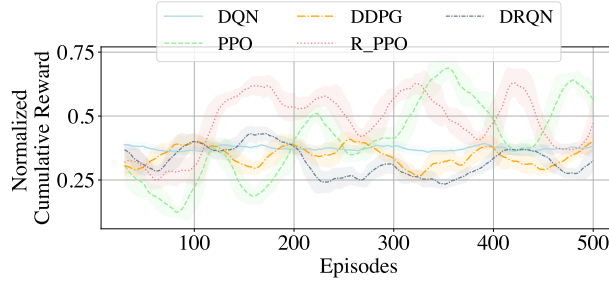


Figure 5: Cumulative reward progression over 500 episodes for agents initially trained on Chameleon Cloud nodes with throughput focused energy objective (T/E) reward signal and subsequently tuned on Cloudfab nodes. The plot illustrates the improvement in cumulative rewards per episode during the tuning process, with each line representing a different agent and shaded areas indicating the variability of the achieved rewards.

3.7 SPARTA Models

We train two SPARTA variants, both employing the R_PPO algorithm but differing in their reward functions as detailed in Section 3.3.3. Specifically:

- **SPARTA-FE:**
This model adopts the *Fairness and Efficiency* objective (F&E Reward), as defined in Eq. 4. By penalizing excessive packet loss, it promotes balanced bandwidth sharing among competing flows, thereby reducing congestion and indirectly lowering energy waste. As discussed in Section 3.3.3, this reward function encourages higher throughput while mitigating congestion-related inefficiencies.
- **SPARTA-T:**
This variant targets the *Throughput-Focused Energy Efficiency* objective (T/E Reward) presented in Eq. 5. It explicitly prioritizes maximizing throughput per unit energy consumed by adapting concurrency and parallelism to conserve energy without sacrificing acceptable performance. The energy-based reward formulation in Section 3.3.3 guides the agent to achieve this balance.

Both models share the same state-space design and R_PPO training framework (see Section 3.6), differing only in their reward functions. This flexibility allows network operators to select the SPARTA variant that best aligns with their specific performance and energy-efficiency requirements.

4 Evaluation

We assess the performance of SPARTA and compare it with state-of-the-art solutions on multiple testbeds (i.e., CloudLab, Chameleon Cloud, and FABRIC) with different network configurations, measuring throughput, energy consumption, and fairness. In each trial, we send $1000 \times 1\text{GB}$ files from a dedicated sender to a receiver. We repeat the entire transfer procedure five times in sequence, collecting performance and resource usage metrics for each run. Our results are shown as distributions aggregated from these five trials.

We compare two static tools (`rc1one` and `escp`), an online optimizer (`Falcon_MP` [15]), a historical-data-driven method called 2-phase [11], and our two DRL-based approaches, (SPARTA-T and SPARTA-FE). The 2-phase model typically mines prior historical data to guide parameter tuning in real time, but because we did not have historical datasets in our testbed setup, we initialized it from a midpoint range of concurrency (cc) and parallelism (p). For both DRL SPARTA agents, we initially set cc and p at a midpoint within the concurrency/parallelism range. If prior knowledge about promising throughput at certain settings is available, these initial values can instead be chosen accordingly. Meanwhile, `Falcon_MP` starts from a baseline configuration and uses gradient descent to tune concurrency and parallelism, while `rc1one` and `escp` maintain the same parameters for the duration of each session.

4.1 Experimental Setup

We conduct experiments on three distinct cloud environments with different network connectivity to illustrate the effectiveness of our approach:

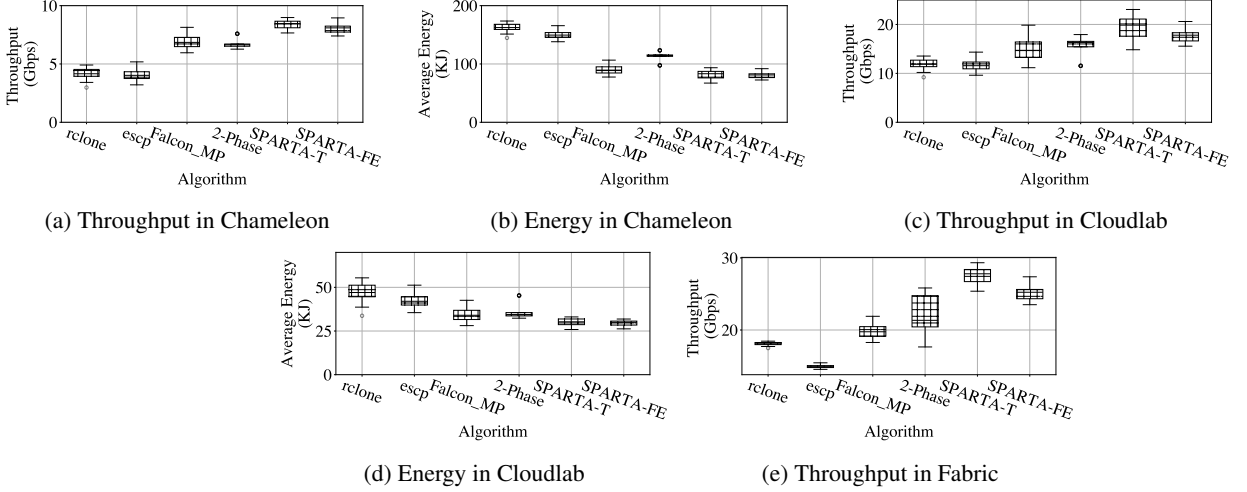


Figure 6: Throughput and energy usage in Chameleon, CloudLab, and FABRIC (1 TB of 1 GB files) using six methods: `rclone`, `escp`, `Falcon_MP`, `2-phase`, `SPARTA-T` and `SPARTA-FE`. The static tools (`rclone`, `escp`) fix $(cc, p) = (4, 4)$, while `Falcon_MP` updates (cc, p) via gradient descent from a baseline. `SPARTA-T` and `SPARTA-FE` build on reinforcement learning. `2-phase` typically uses historical logs, but here starts from midpoint settings in the absence of extensive data. Due to a lack of hardware counters in FABRIC, only throughput is reported for that testbed.

Chameleon Cloud: We deploy the sender and receiver on `gpu_p100` nodes at TACC, featuring Intel Xeon E5-2670 v3 processors (2 CPUs, 48 threads total), 128 GiB RAM, and two NVIDIA P100 GPUs. Each node also includes 400–1000 GB of local storage and a 10 Gbps NIC (Broadcom NetXtreme II BCM57800). The WAN path between TACC and the University of Chicago sites is shared and can support up to 10 Gbps of throughput.

CloudLab: Our experiments here utilized two node types: `c6525-100g` (Utah Site): AMD EPYC 7402P with 48 cores @2.8 GHz, 128 GB RAM, 3200 GB local disk, and a 25 Gbps NIC (bandwidth externally capped at 25 Gbps). `d7525` (Wisconsin Site): AMD EPYC 64 cores @3.0 GHz, 128 GB RAM, 2560 GB local disk, and a 200 Gbps NIC (again limited to 25 Gbps for the WAN). We place the sender and receiver at Utah and Wisconsin, respectively, to create a wide-area transfer scenario.

FABRIC: We use virtual machine (VM) instances at the Princeton and Utah sites, each equipped with 32 CPU cores, 128 GB of RAM, and 2560 GB of disk. Each VM accesses a `ConnectX_6` 100 Gbps NIC, though the effective WAN bandwidth was near 30 Gbps. Because these are virtualized environments, no direct hardware counters are available for energy measurements. Consequently, we only report throughput for FABRIC experiments.

All transfers are performed using Apache servers on the sender side and memory-to-memory transfers at the destination, with TCP CUBIC as the transport protocol across all sites. In Chameleon and CloudLab, we measure energy consumption using Intel’s Running Average Power Limit (RAPL) [9], subtracting each system’s baseline power to isolate the energy used for data transfers. Since FABRIC lacks direct hardware counters for energy measurements, we only report throughput.

4.2 Performance Across Testbeds

Figure 6 summarizes throughput and energy usage at the Chameleon Cloud and CloudLab, and throughput only at the FABRIC testbeds.

`rclone` and `escp` rely on static $(cc, p) = (4, 4)$ configuration, averaging around 4–6 Gbps transfer throughput. `Falcon_MP`, which starts from a baseline and uses gradient descent, reaches about 8 Gbps after multiple iterations. `SPARTA-T` and `SPARTA-FE` adapt their parameters more flexibly, often hitting 9–10 Gbps. Meanwhile, `2-phase`, which depends on extensive historical logs to guide parameter choices, could not fully exploit its offline modeling here and thus settles near 7 Gbps.

`rclone` and `escp` exhibit relatively high energy usage due to underutilized link capacity resulting in prolonged transfer time. `Falcon_MP` does better than `rclone` and `escp` due to improved throughput and smaller transfer time. `SPARTA-T` and `SPARTA-FE` maintains the lowest energy expenditure by directly optimizing for throughput-to-energy

ratios. 2-phase remains in a mid-range energy profile, reflecting its partial adaptation without an extensive historical dataset.

4.2.1 CloudLab (Figures 6c and 6d)

Constrained by a 25 Gbps link, SPARTA-T and SPARTA-FE each manage 22–24 Gbps transfer throughput on average, surpassing `rc1one` and `escp` (16–18 Gbps). `Falcon_MP` again requires multiple steps to approach 20 Gbps. Lacking its usual historical data, 2-phase settles near 14 Gbps, trailing both the DRL based SPARTA agents.

SPARTA-FE continues to post the lowest energy usage, validating its energy-aware reward function. SPARTA-T uses slightly more energy compared to SPARTA-FE. 2-phase shows moderate energy consumption in the absence of extensive logs, while `Falcon_MP`, starting from a baseline, experiences longer convergence and resulting higher energy usage.

4.2.2 FABRIC (Figure 6e)

No hardware counters for energy measurement are available in FABRIC, so we only report the transfer throughput. Despite a nominal 100 Gbps link and a 56 ms RTT, practical factors such as shared NIC among VMs limit attainable average throughput to roughly 28 Gbps (Figure 6e). Within these bounds, both DRL SPARTA methods achieve 20–25 Gbps, while `Falcon_MP` converges more slowly. 2-phase also lags behind the DRL based SPARTA agents due to lack of historical transfer data.

Overall, the DRL-based SPARTA agents outperform static, online optimizers and methods dependent on transition logs (`rc1one`, `escp`, `Falcon_MP`, 2-phase) by continuously adjusting concurrency (cc) and parallelism (p) in near real time. In particular, SPARTA-FE achieves a lower overall energy footprint but delivers slightly less throughput compared to SPARTA-T. This difference arises because SPARTA-FE includes packet loss rate directly in its reward signal, making it more conservative; it reacts quickly to congestion by reducing parameters to avoid excessive packet loss and ensure fair bandwidth allocation. In contrast, SPARTA-T relies on the throughput-to-energy ratio, which typically drops only after throughput has already decreased (often following packet loss), so it has more time to maintain higher throughput—even though this leads to increased energy usage. Meanwhile, `Falcon_MP` needs multiple gradient-descent steps from its baseline to converge, and 2-phase, which typically exploits extensive historical logs, cannot fully leverage its modeling without such data—leading both to lag behind the DRL-based SPARTA agents. These results underscore the advantages of learning-based, multi-parameter adaptation in high-bandwidth, dynamic network environments.

4.3 Fairness in Concurrent Transfers

In many real-world deployments, multiple data flows share the same bottleneck link, making fairness essential for efficient resource allocation. To assess this, we launch concurrent transfers using different optimizers. Figures 7a, 7b, and 7c show three representative scenarios:

- (a) Three transfers running SPARTA-T *Throughput-Focused Energy Efficiency* objective (T/E Reward, see Eq. 5).
- (b) Three transfers running SPARTA-FE *Fairness and Efficiency* objective (F&E Reward, see Eq. 4).
- (c) A mixed scenario with one transfer each using SPARTA-FE, `Falcon_MP`, and `rc1one`.

4.3.1 Jain’s Fairness Index (JFI)

We quantify fairness using Jain’s Fairness Index (JFI) [56], which measures how evenly bandwidth is distributed among n concurrent flows with throughputs $\{T_1, T_2, \dots, T_n\}$:

$$\text{JFI} = \frac{(\sum_{k=1}^n T_k)^2}{n \sum_{k=1}^n (T_k)^2}. \quad (18)$$

A JFI close to 1 indicates nearly perfect fairness; lower values signify larger throughput imbalances among flows.

4.3.2 SPARTA-T (T/E Reward) Fairness (Figure 7a)

We begin by running three concurrent transfers using SPARTA-T, which implements the *Throughput-Focused Energy Efficiency* (T/E) Reward (see Section 3.3.3). As each flow seeks to maximize its throughput-to-energy ratio, they converge to different throughput levels depending on arrival times. Consequently, the overall Jain’s Fairness Index (JFI) remains moderate because the T/E Reward does not heavily penalize bandwidth imbalances. Moreover, SPARTA-T can

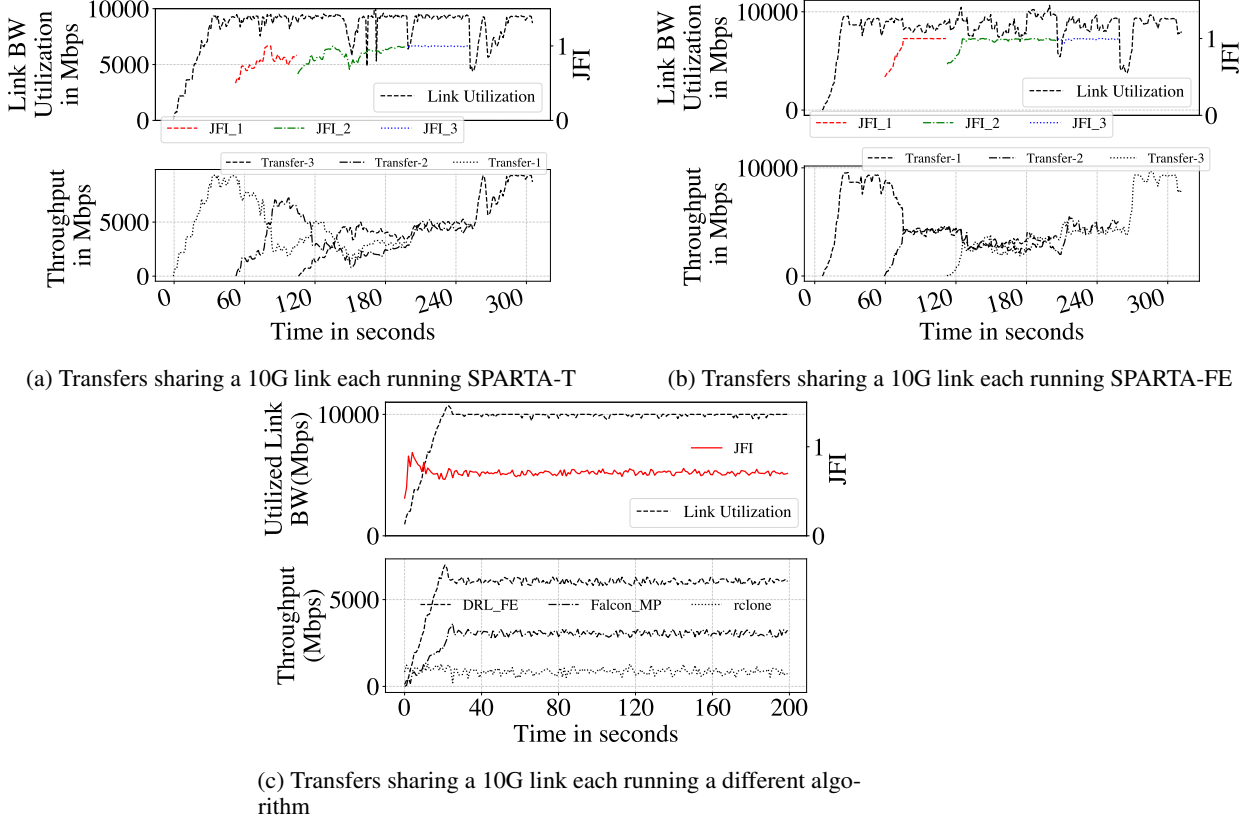


Figure 7: Comparison of transfer performance in Chameleon cloud between TACC and UC sites. (a) Shows three transfers running separate SPARTA-T for a 10G shared link. (b) Shows three transfers running separate SPARTA-FE with the same shared environment. SPARTA-FE achieves better fairness compared to SPARTA-T because of the inclusion of packet loss rate in the reward function, which makes SPARTA-FE share the available resources more fairly.

show larger fluctuations in JFI when multiple flows share the network, since it adjusts concurrency and parallelism primarily to optimize throughput per energy. Once a flow completes or detects diminishing energy returns, other flows opportunistically claim the freed capacity, yielding strong per-bit energy savings but potentially fluctuate fairness score among simultaneous transfers.

4.3.3 SPARTA-FE (F&E Reward) Fairness (Figure 7b)

Next, we repeat the three-transfer experiment with SPARTA-FE, which employs the *Fairness and Efficiency* (F&E) Reward. This reward explicitly factors in packet loss to enforce fairness while also indirectly reducing wasted energy from congestion. After a brief exploration phase, all flows converge to an equal share of the link, yielding a significantly higher JFI. When any flow ends, the remaining flows dynamically scale their parameters to use the newly available bandwidth, while still preventing congestion. Because packet loss directly impacts the F&E Reward, SPARTA-FE responds faster to incipient congestion than T/E-based approaches, resulting in more stable fairness when multiple flows are active.

4.3.4 Mixed Algorithms Fairness (Figure 7c)

Finally, we test a scenario with three concurrent data transfers, each using a different approach:

- SPARTA-FE (F&E Reward),
- Falcon_MP (online concurrency/parallelism tuning via gradient descent),
- rclone (static concurrency=4, parallelism=4).

In Figure 7c, SPARTA-FE and Falcon_MP both start from similar parameter settings. However, SPARTA-FE quickly and intelligently adjusts (cc, p) , achieving high throughput sooner. As Falcon_MP gradually ramps up its concurrency,

SPARTA-FE reduces its own parameters slightly to accommodate the new flows. By contrast, `rc1one` remains at its baseline setting. Overall, the JFI remains high, indicating that SPARTA-FE maintains a balanced share of the link after convergence.

In summary, SPARTA-T optimizes throughput per unit energy, sometimes allowing throughput imbalances to persist. Conversely, SPARTA-FE factors packet loss directly into its reward, actively discouraging congestion and achieving higher fairness across flows. Even in the mixed scenario, SPARTA-FE adapts its parameters to accommodate incoming flows or reclaim unused capacity, resulting in consistently higher JFI than T/E-based or static approaches.

5 Conclusion

In this paper, we present SPARTA, a multi-parameter deep reinforcement learning (DRL) framework that automatically tunes concurrency (cc) and parallelism (p) to boost data transfer performance in high-speed networks. Using real-world state transition data, we design two agent variants: SPARTA-T with a *throughput-focused energy efficiency (T/E) reward* and SPARTA-FE with a *fairness and efficiency (F&E) Reward*. These reward signals enable the agents to balance throughput with energy usage while ensuring fair bandwidth sharing. Tested on multiple testbeds, SPARTA consistently outperforms both baseline and state-of-the-art methods, requiring only minimal configuration and showcasing the advantages of adaptive resource allocation.

SPARTA trains DRL agents using energy- and fairness-aware reward signals, allowing them to pause and resume transfer threads based on real-time network conditions. This flexibility not only speeds up data transfers but also prevents overloading resources and lowers energy use. To speed up training, we introduce an emulation environment that stores transition logs from initial real-world training episodes. By learning from these logs, the agents quickly discover optimal actions without the high costs of lengthy real-world transfers. After training, they intelligently adjust cc and p to avoid resource congestion during busy periods and to fully use available bandwidth during quieter times, all without sacrificing fairness.

Although our experiments focus on multiple concurrent transfers on shared links, future work could scale this approach to hundreds or even thousands of transfers across geographically distributed environments. This might involve multi-agent DRL or centralized optimization strategies and also incorporate other transport protocol such as TCP BBR [23].

In summary, our results show that DRL-based resource allocation can build more sustainable, high-performing data transfer infrastructures that save energy, increase throughput, and maintain fairness.

References

- [1] Global IP Traffic Forecast and Methodology, 2018–2023 (White Paper). Cisco Systems, 2023.
- [2] Internet2. Internet2. <https://internet2.edu>. Accessed: 2025-01-23.
- [3] ESnet. Energy Sciences Network (ESnet). <https://www.es.net>. Accessed: 2025-01-23.
- [4] Mehmet Balman and Tevfik Kosar. Data scheduling for large scale distributed applications. In *the 5th ICEIS Doctoral Consortium, In conjunction with the International Conference on Enterprise Information Systems (ICEIS'07)*. Funchal, Madeira-Portugal, 2007.
- [5] Luigi Di Tacchio, MD S Q Zulkar Nine, Tevfik Kosar, Muhammed Fatih Bulut, and Jinho Hwang. Cross-layer optimization of big data transfer throughput and energy consumption. In *2019 IEEE CLOUD*, 2019.
- [6] Suresh Marru, Brian Freitag, Dimuthu Wannipurage, Uday Kumar Bommala, Patrick Pradier, Christophe Demange, Nishan Pantha, Tathagata Mukherjee, Betlem Rosich, Eric Monjoux, and Rahul Ramachandran. Blaze: A high-performance, scalable, and efficient data transfer framework with configurable and extensible features : Principles, implementation, and evaluation of a transatlantic inter-cloud data transfer case study. In *2023 IEEE 16th International Conference on Cloud Computing (CLOUD)*, pages 58–68, 2023.
- [7] Paras Jain, Sam Kumar, Sarah Wooders, Shishir G. Patil, Joseph E. Gonzalez, and Ion Stoica. Skyplane: Optimizing transfer cost and throughput using Cloud-Aware overlays. In *20th USENIX Symposium on Networked Systems Design and Implementation (NSDI 23)*, pages 1375–1389, Boston, MA, April 2023. USENIX Association.
- [8] Ladislav Pápay, Jan Pustelnik, Krzysztof Rzadca, Beata Strack, Paweł Stradomski, Bartłomiej Wołowiec, and Michał Zasadzinski. An exabyte a day: throughput-oriented, large scale, managed data transfers with effingo. In *Proceedings of the ACM SIGCOMM 2024 Conference*, ACM SIGCOMM '24, page 970–982, New York, NY, USA, 2024. Association for Computing Machinery.

- [9] Hasibul Jamil, Lavone Rodolph, Jacob Goldverg, and Tevfik Kosar. Energy-efficient data transfer optimization via decision-tree based uncertainty reduction. In *ICCCN*, pages 1–10, 2022.
- [10] Lavone Rodolph, MD S Q Zulkar Nine, Luigi Di Tacchio, and Tevfik Kosar. Energy-saving cross-layer optimization of big data transfer based on historical log analysis. In *IEEE ICC 2021*, pages 1–7, 2021.
- [11] MD S Q Zulkar Nine and Tevfik Kosar. A two-phase dynamic throughput optimization model for big data transfers. *IEEE Transactions on Parallel and Distributed Systems*, 32(2):269–280, 2021.
- [12] Dong Lu, Yi Qiao, P.A. Dinda, and F.E. Bustamante. Modeling and taming parallel tcp on the wide area network. In *IPDPS*, 2005.
- [13] Esmay Yildirim, Engin Arslan, Jangyoung Kim, and Tevfik Kosar. Application-level optimization of big data transfers through pipelining, parallelism and concurrency. *IEEE Trans. Cloud Comput.*, 4(1):63–75, January 2016.
- [14] Md Arifuzzaman and Engin Arslan. Online optimization of file transfers in high-speed networks. In *Proceeding of Super*. ACM, 2021.
- [15] Md Arifuzzaman, Brian Bockelman, James Basney, and Engin Arslan. Falcon: Fair and efficient online file transfer optimization. *IEEE Transactions on Parallel and Distributed Systems*, 34(8):2265–2278, 2023.
- [16] Lotfi Belkhir and Ahmed Elmeligi. Assessing ict global emissions footprint: Trends to 2040 & recommendations. *Journal of cleaner production*, 177:448–463, 2018.
- [17] Anders SG Andrae and Tomas Edler. On global electricity usage of communication technology: trends to 2030. *Challenges*, 6(1):117–157, 2015.
- [18] Clarisse Aujoux, Kumiko Kotera, and Odile Blanchard. Estimating the carbon footprint of the grand project, a multi-decade astrophysics experiment. *Astroparticle Physics*, 131:102587, 2021.
- [19] Ismail Alan, Engin Arslan, and Tevfik Kosar. Energy-aware data transfer algorithms. In *SC '15: Proceedings of the International Conference for High Performance Computing, Networking, Storage and Analysis*, pages 1–12, 2015.
- [20] Hasibul Jamil, Elvis Rodrigues, Jacob Goldverg, and Tevfik Kosar. Learning to maximize network bandwidth utilization with deep reinforcement learning. In *GLOBECOM 2023 - 2023 IEEE Global Communications Conference*, pages 3711–3716, 2023.
- [21] Chen Tessler, Yuval Shpigelman, Gal Dalal, Amit Mandelbaum, Doron Haritan Kazakov, Benjamin Fuhrer, Gal Chechik, and Shie Mannor. Reinforcement learning for datacenter congestion control. *CoRR*, abs/2102.09337, 2021.
- [22] Wei Li, Fan Zhou, Kaushik Roy Chowdhury, and Waleed Meleis. Qtcp: Adaptive congestion control with reinforcement learning. *IEEE Transactions on Network Science and Engineering*, 6(3):445–458, 2019.
- [23] Neal Cardwell, Yuchung Cheng, C. Stephen Gunn, Soheil Hassas Yeganeh, and Van Jacobson. Bbr: Congestion-based congestion control: Measuring bottleneck bandwidth and round-trip propagation time. *Queue*, oct 2016.
- [24] Mo Dong, Tong Meng, Doron Zarchy, Engin Arslan, Yossi Gilad, Brighten Godfrey, and Michael Schapira. PCC vivace: Online-Learning congestion control. In *NSDI 18*, Renton, WA, 2018.
- [25] Bryce Allen, John Bresnahan, Lisa Childers, Ian Foster, Gopi Kandaswamy, Raj Kettimuthu, Jack Kordas, Mike Link, Stuart Martin, Karl Pickett, and Steven Tuecke. Software as a service for data scientists. *Commun. ACM*, 55(2):81–88, February 2012.
- [26] Daqing Yun, Chase Q. Wu, Nageswara S. V. Rao, and Rajkumar Kettimuthu. Advising big data transfer over dedicated connections based on profiling optimization. *IEEE/ACM Transactions on Networking*, 27(6):2280–2293, 2019.
- [27] David Brooks, Vivek Tiwari, and Margaret Martonosi. Wattch: a framework for architectural-level power analysis and optimizations. In *Proceedings of the 27th annual international symposium on Computer architecture*, ISCA '00, pages 83–94, New York, NY, USA, 2000. ACM.
- [28] Freeman Rawson and IBM Austin. Mempower: A simple memory power analysis tool set. *IBM Austin Research Laboratory*, 2004.
- [29] John Zedlewski, Sumeet Sobti, Nitin Garg, Fengzhou Zheng, Arvind Krishnamurthy, and Randolph Y Wang. Modeling hard-disk power consumption. In *FAST 2003*.
- [30] Sudhanva Gurusurthi, Anand Sivasubramaniam, Mary Jane Irwin, Narayanan Vijaykrishnan, and Mahmut Kandemir. Using complete machine simulation for software power estimation: The softwatt approach. In *Prpc. of 8th High-Performance Computer Architecture Symp.*, pages 141–150, 2002.

- [31] Gilberto Contreras and Margaret Martonosi. Power prediction for intel xscale® processors using performance monitoring unit events. In *ISLPED'05*, pages 221–226, 2005.
- [32] Dimitris Economou, Suzanne Rivoire, Christos Kozyrakis, and Partha Ranganathan. Full-system power analysis and modeling for server environments. In *Proc. of Workshop on Modeling, Benchmarking, and Simulation*, 2006.
- [33] Xiaobo Fan, Wolf-Dietrich Weber, and Luiz Andre Barroso. Power provisioning for a warehouse-sized computer. *ACM SIGARCH Computer Architecture News*, 35(2):13–23, 2007.
- [34] Suzanne Rivoire, Parthasarathy Ranganathan, and Christos Kozyrakis. A comparison of high-level full-system power models. *HotPower*, 8:3–3, 2008.
- [35] Ricardo Koller, Akshat Verma, and Anindya Neogi. Wattapp: an application aware power meter for shared data centers. In *Proceedings of the 7th international conference on Autonomic computing*, pages 31–40. ACM, 2010.
- [36] Koji Hasebe, Tatsuya Niwa, Akiyoshi Sugiki, and Kazuhiko Kato. Power-saving in large-scale storage systems with data migration. In *IEEE CloudCom 2010*.
- [37] Susan V Vrbsky, Michael Galloway, Robert Carr, Rahul Nori, and David Grubic. Decreasing power consumption with energy efficient data aware strategies. *FGCS*, 29(5):1152–1163, 2013.
- [38] G. Ananthanarayanan and R. Katz. Greening the switch. In *In Proceedings of HotPower, December 2008*.
- [39] P. Mahadevan, P. Sharma, S. Banerjee, and P. Ranganathan. A power benchmarking framework for network devices. In *In Proceedings of IFIP Networking, May 2009*.
- [40] A. Greenberg, J. Hamilton, D. Maltz, and P. Patel. The cost of a cloud: Research problems in data center networks. In *In ACM SIGCOMM CCR, January 2009*.
- [41] Md SQ Zulkar Nine, Tevfik Kosar, Muhammed Fatih Bulut, and Jinho Hwang. Greenfv: Energy-efficient network function virtualization with service level agreement constraints. In *Proceedings of the International Conference for High Performance Computing, Networking, Storage and Analysis*, pages 1–12, 2023.
- [42] Ismail Alan, Engin Arslan, and Tevfik Kosar. Energy-aware data transfer algorithms. In *Proceedings of the International Conference for High Performance Computing, Networking, Storage and Analysis*, pages 1–12, 2015.
- [43] Kemal Guner and Tevfik Kosar. Energy-efficient mobile network i/o. In *2018 IEEE Global Communications Conference (GLOBECOM)*, pages 1–6. IEEE, 2018.
- [44] Kate Keahey, Jason Anderson, Zhuo Zhen, and et al. Lessons learned from the chameleon testbed. In *Proceedings of USENIX ATC'20*, July 2020.
- [45] Sangtae Ha, Injong Rhee, and Lisong Xu. Cubic: A new tcp-friendly high-speed tcp variant. volume 42, page 64–74, New York, NY, USA, jul 2008. Association for Computing Machinery.
- [46] Matthew Mathis, Jeffrey Semke, Jamshid Mahdavi, and Teunis Ott. The macroscopic behavior of the tcp congestion avoidance algorithm. volume 27, page 67–82, New York, NY, USA, jul 1997. Association for Computing Machinery.
- [47] T.J. Hacker, B.D. Athey, and B. Noble. The end-to-end performance effects of parallel tcp sockets on a lossy wide-area network. In *IPDPS*, 2002.
- [48] Nathan Jay, Noga Rotman, Brighten Godfrey, Michael Schapira, and Aviv Tamar. A deep reinforcement learning perspective on internet congestion control. In *Proceedings of ICML*, volume 97, pages 3050–3059, 09–15 Jun 2019.
- [49] John Schulman, Filip Wolski, Prafulla Dhariwal, Alec Radford, and Oleg Klimov. Proximal policy optimization algorithms. arXiv:1707.06347, 2017.
- [50] Steven Kapturowski, Georg Ostrovski, John Quan, Rémi Munos, and Will Dabney. Recurrent experience replay in distributed reinforcement learning. In *International Conference on Learning Representations (ICLR)*, 2019.
- [51] Timothy P. Lillicrap, Jonathan J. Hunt, Alexander Pritzel, Nicolas Heess, Tom Erez, Yuval Tassa, David Silver, and Daan Wierstra. Continuous control with deep reinforcement learning. arXiv:1509.02971, 2016.
- [52] V. Mnih, K. Kavukcuoglu, D. Silver, and et al. Human-level control through deep reinforcement learning. *Nature*, 518:529–533, February 2015.
- [53] Matthew J. Hausknecht and Peter Stone. Deep recurrent q-learning for partially observable mdps. In *2015 AAAI Fall Symposium Series*, 2015.
- [54] Stuart P. Lloyd. Least squares quantization in PCM. *IEEE Transactions on Information Theory*, 28(2):129–137, 1982.

- [55] Nicolas Heess, Greg Wayne, David Silver, Timothy Lillicrap, Yuval Tassa, and Tom Erez. Memory-based control with recurrent neural networks. In *NIPS Deep Reinforcement Learning Workshop*, 2015.
- [56] R. Jain, D. Chiu, and W. Hawe. A quantitative measure of fairness and discrimination for resource allocation in shared computer systems, 1998.

APPENDIX

Below, we present the key hyperparameters used for each RL algorithm evaluated in our study. These tables provide details on network architectures, learning rates, batch sizes, and other parameters tailored to optimize concurrency (cc) and parallelism (p) under various performance objectives. All tables in this appendix follow the same format, listing each hyperparameter and its corresponding value.

Table 2: DQN Hyper-parameters

Hyperparameter	Value
Model type	fully-connected
Activation function	ReLU
Buffer size	10000
Model hidden layers	[128, 128]
Batch size	32
Train frequency	4
Update interval	1000
Exploration fraction	0.1
Final epsilon	0.02
Max gradient norm	10

Table 3: PPO Hyper-parameters

Hyperparameter	Value
Model type	fully-connected
Learning rate	0.0003
Activation function	ReLU
Number of steps	2048
Batch size	64
Policy hidden layers	[128, 128]
Value function hidden layers	[128, 128]
Number of epochs	10
Gamma	0.99
GAE lambda	0.95
Clip range	0.2
Entropy coefficient	0.0
Value function coefficient	0.5
Max gradient norm	0.5
Normalize advantage	true
Use SDE	false

Table 4: DDPG Hyper-parameters

Hyperparameter	Value
Model type	fully-connected
Learning rate	0.001
Activation function	ReLU
Buffer size	1000000
Model hidden layers	[400, 300]
Learning starts	100
Batch size	256
Tau	0.005
Gamma	0.99
Train frequency	1
Gradient steps	1
Action noise	None

Table 5: Recurrent PPO Hyper-parameters

Hyperparameter	Value
Model type	Recurrent fully-connected
Learning rate	0.0003
Activation function	Tanh
LSTM hidden size	256
Batch size	128
Number of LSTM layers	1
Number of epochs	10
Enable critic LSTM	True
Gamma	0.99
GAE lambda	0.95
Clip range	0.2
Value function coefficient	0.5
Entropy coefficient	0.0
Max gradient norm	0.5
Normalize advantage	True
Use SDE	False

Table 6: DRQN Hyper-parameters

Hyperparameter	Value
Model type	Recurrent fully-connected
Learning rate	0.001
Activation function	ReLU
Buffer size	1000000
Model hidden layers	[64, LSTM(64)]
Learning starts	100
Batch size	256
Target update period	4
Gamma	0.99
Tau	0.01
Episodes	500000
Epsilon start	0.1
Epsilon end	0.001
Epsilon decay	0.995
Max episode length	128
Random update	True